

Probing AGN Disks Density Profiles through Gravitational Wave Observations

Xiangyu Lyu, En-Kun Li, Changfu Shi,* and Yi-Ming Hu†

MOE Key Laboratory of TianQin Mission, TianQin Research Center for Gravitational Physics & School of Physics and Astronomy, Frontiers Science Center for TianQin, Gravitational Wave Research Center of CNSA, Sun Yat-sen University (Zhuhai Campus), Zhuhai 519082, China

Massive black holes surrounded by a gaseous disk have been a prevailing model to explain a wide spectrum of astrophysical phenomena related to active galactic nuclei (AGNs). However, direct and precise measurements of the disk density profiles remain elusive for current telescopes. In this work, we demonstrate that it is possible to pinpoint the gas density if an inspiralling stellar mass binary black hole is embedded in the AGN disk. Furthermore, if the barycenter of the pair follows an eccentric orbit around an AGN, then space-borne gravitational wave detectors can measure the density of the surrounding disk with multi-year observations by tracking the gravitational wave evolution. The error between the inferred density profile and the injected truth can be constrained to below $2 \times 10^{-11} \text{ g/cm}^3$. Our work opens up an exciting new channel to investigate the very center of galaxies, where disk gas density distributions $\rho(r)$ can be recovered by analyzing time-dependent environmental imprints in gravitational waveforms.

Introduction. – Powered by the gas accretion onto central supermassive black holes (SMBHs), AGN system is one of the most luminous objects in the universe [1]. Accretion disks in AGNs serve as the complex engine surrounding central SMBHs, which is vital in researching the coupled evolution of galaxies and central SMBHs [2, 3]. Numerous efforts have been made to uncover the real structure of the AGN disk, for example, the direct observation from Event Horizon Telescope (EHT) [4, 5], very long baseline interferometry (VLBI) [6] and other ultraviolet/optical continuous spectrum observations [7–11]. However, either the resolution or the detection distances of the above electromagnetic (EM) observation methods is inadequate for studying the central regions of AGNs [4, 5]. Thus, research on accretion disks necessitates new observational approaches.

With the operation of ground-based Gravitational wave (GW) detectors, the recent decade has witnessed a revolutionary breakthrough in exploring the dark universe. It has been proposed that stellar mass binary black hole (sBBH) could form and merge in disks [12–15]. For example, The LIGO-Virgo-KAGRA (LVK) collaboration has observed sBBH systems with masses lying in the mass gap [16–22], like GW190521 [23] and GW190426_190642 [24]. The most recent observation GW231123 [25] even comprises two component black holes (BHs) heavier than $100 M_\odot$. These observations provide strong support for hierarchical mergers, which most likely originate from dynamically active regions, such as the AGN disks. Besides, Graham et al. [26] reported that GW190521 [27] could be accompanied by an EM counterpart in an AGN system. These sBBHs’ GW waveforms will encode environmental signatures reflecting disk properties. For example, the gas density and the SMBH mass [28–30] can be recovered by the corresponding GW phase modification by gas accretion [31], dynamical friction (DF) from surrounding gas [32], and binary’s center of mass (CoM) acceleration from the third

body [33–36]. In conclusion, GW observation is an essential tool for directly measuring the environmental properties. However, until now, LVK haven’t found robust evidence supporting the environmental effects in the detected GW signals. This absence indicates that the most extreme ambient gas densities ($\geq 10^7 \text{ g/cm}^3$) have been ruled out for these systems [37, 38].

The space-borne GW detectors can observe the early inspiral of the sBBH months to years before these systems enter the high-frequency band ($\geq 10 \text{ Hz}$) [39, 40]. They can also measure the parameters of the binaries to very high precision: chirp mass $\Delta M_c/M_c \sim 10^{-7}$, sky localization $\sim 1 \text{ deg}^2$, and coalescence time errors $\sim 1 \text{ s}$ [39–46], which facilitates host galaxy identification and enables early warnings for EM follow-up observations [39, 40, 47]. Besides, parameter of disks like gas density ρ can be well constrained that $\delta\rho \sim 10^{-10} \text{ g/cm}^3 - 10^{-12} \text{ g/cm}^3$ [29–31]. We remark that previous studies assume a stable environment, and only local properties of the disk can be recovered.

By adopting the thin disk model [48, 49], the gas density ρ decreases with larger radial distance r to AGN center $\rho \propto r^{-3}$. This means that if the barycenter of sBBH moves around the AGN center on an eccentric orbit, these systems may experience the variation of the density $\Delta\rho$. The X-ray observation of the quasiperiodic eruptions (QPEs) often reports a “long-short” pattern for the recurrence time, and some suspect that compact objects that follow an eccentric orbit around the massive black holes might just explain this [50, 51].

In this letter, we demonstrate that space-borne detectors, such as TianQin, can achieve high-precision constraints on the density profile of the AGN accretion disk through sBBH GW observations. We show that, under the assumption that the barycenter of the sBBH follows an eccentric orbit, the parameter estimation results for the environment density are precise enough to distinguish the inherent gas density variation over three-month ob-

servational intervals, and the profile of the disk can be determined with sequential observations. In this study, we employ a natural unit system with $c = G = 1$.

Capability of constraining environmental effect by sBBH systems. –

sBBHs will experience DF effect throughout their evolution if embedded in a dense environment (e.g., accretion disk or dark matter halo), while the environment could imprint detectable signatures on GW signals. This effect exerts a drag force on component BH, introducing a -5.5 post-Newtonian order phase correction to the waveform [31, 52–54]:

$$\tilde{\phi}_{\text{DF}} \simeq -\rho \frac{25\pi(3\eta-1)M_z^2}{739328\eta^2} \gamma_{\text{DF}} [\pi f M_z]^{-16/3}, \quad (1)$$

where ρ is the ambient density, $M_z = M_c(1+z)$ is the redshifted chirp mass of sBBH system, η is the systematic mass ratio, γ_{DF} is the relative DF effect parameter [29].

In our analysis, we adopted a GW190521-like sBBH as the fiducial system with the source parameters $\boldsymbol{\theta} = \{D_L, M_c, \eta, \chi_1, \chi_2, \iota, t_c, \phi_c\}$ chosen as: luminosity distance $D_L = 1000\text{Mpc}$, chirp mass $M_c = 77.66M_\odot$, systematic mass ratio $\eta = 0.23$, aligned spin ($\chi_1 = 0.80, \chi_2 = 0.80$), inclination angle $\iota = \pi/6$, coalescence phase $\phi_c = 0$, and coalescence time $t_c = 5\text{yrs}$. The DF effect parameter $\gamma_{\text{DF}} = -247 \log \left[\frac{f}{c_s/(22\pi M)} \right] - 39 + 304 \log 20 + 38 \log \frac{3125}{8}$ is related with the gas sound speed c_s and total mass M , which was set to be 0.02 and $155.60M_\odot$. We neglected the sky location and polarization angle and instead used the sky-averaged TianQin antenna pattern function [40] and the IMRPhenomPv2 [55] waveform. Specially, TianQin has a “3 month on, 3 month off” observation schedule [56], however, for the purpose of demonstration, we assume a 5yr continuous observation ($T_{\text{orb}} = 5\text{yrs}$), and the observation data \mathbf{D} compose of 20 segments $[D_1, D_2, \dots, D_{20}]$. Based on the fiducial system, we adopted the same environment density $\rho = 10^{-10}\text{g/cm}^3$ in Toubiana et al. [29] as the injected value in a three-month simulated GW signal, and we assume this value to be a constant during this period.

To assess capability of TianQin in constraining environmental effect, we first simulate a five-year mock observation data \mathbf{D} , and we do not inject noise to avoid potential bias. Under the aforementioned parameter set $\boldsymbol{\theta}$, the signal to noise ratio (SNR) of the fiducial system is 11.8, which surpasses the detection threshold (SNR=8) of space-borne GW detectors. We then estimate the posterior distribution $P(\boldsymbol{\theta}|D)$ under the Bayesian inference, with the first three-month observation data D_1 . In Bayesian inference, the posterior distribution $P(\boldsymbol{\theta}|D)$ is proportional to the product of the likelihood function $\mathcal{L}(\boldsymbol{\theta})$ and prior $P(\boldsymbol{\theta})$. The logarithm of likelihood $\mathcal{L}(\boldsymbol{\theta})$ can be defined as $\log \mathcal{L}(\boldsymbol{\theta}) \propto -\frac{1}{2}(D - h(\boldsymbol{\theta})|D - h(\boldsymbol{\theta}))$, where $\langle a(t), b(t) \rangle = 4\Re \left[\int_0^\infty df \frac{\tilde{a}(f)\tilde{b}^*(f)}{S_n(f)} \right]$ is the inner

product, with the $S_n(f)$ being the one-sided power spectral density (PSD) [40, 57].

For the Bayesian inference, we adopt the `emcee` implementation [58] of the affine-invariant Markov chain Monte Carlo (MCMC) ensemble sampler. Also use the Fisher information matrix (FIM) method to calculate the precision $\delta\theta$ and therefore estimate the ability of TianQin in constraining the gas density. With the FIM matrix $\Gamma_{ij} = \langle \frac{\partial h}{\partial \theta_i}, \frac{\partial h}{\partial \theta_j} \rangle$, the covariance matrix can be approximated as $\Sigma = \Gamma^{-1}$ [59].

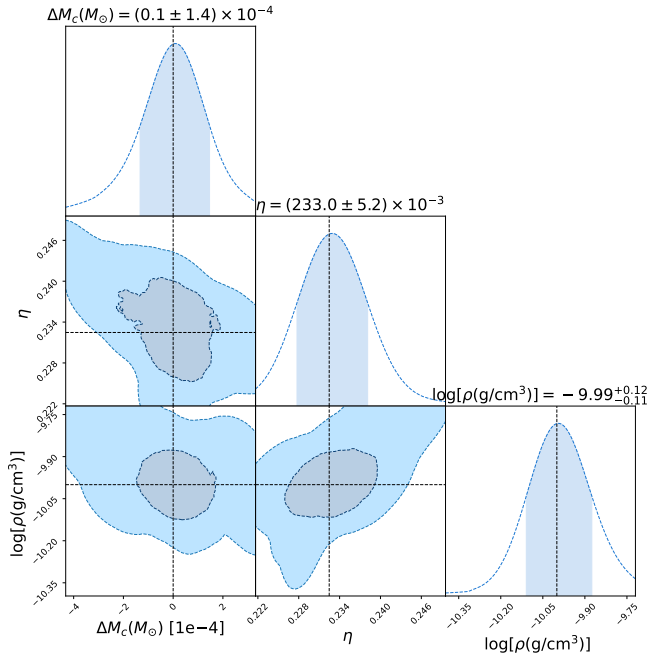


FIG. 1: The posterior distribution of three parameters $\Delta M_c, \eta, \log \rho$ of a GW190521-like system. Black dashed lines represent the injected value, and light blue contour lines are 68% and 95% credible intervals (CI). And subplot headers report central estimates with 1σ uncertainties.

Fig.1 demonstrates the parameter estimation results for (M_c, η, ρ) under three-month observation of TianQin, with all other parameters fixed to the injected values, and (M_c, η, ρ) are the only free parameters, while all other parameters are fixed to their injected values. For clearer visualization, we present the relative deviation in chirp mass $\Delta M_c = M_c - M_c^{\text{inject}}$, and express the environmental density in logarithmic form $\log[\rho/(g/cm^3)]$. Our results reveal that $\rho = 0\text{ g/cm}^3$ is outside the 90%CI region, highlighting the fact that TianQin could decisively detect the environment effect in the GW signal. Furthermore, with three-month observation, TianQin can constrain the environment density to the precision $\delta\rho \sim 10^{-11}\text{g/cm}^3$.

Recovering the disk density profile. – Throughout five-year operational lifetime of TianQin [56], sequential three-month observational segments could provide independent environmental density estimates $[\rho_1 \pm \delta\rho_1, \rho_2 \pm \delta\rho_2, \dots, \rho_{20} \pm \delta\rho_{20}]$. In this study, we assume an AGN ac-

cretion disk as the astrophysical environment for sBBH systems. If the barycenter of the sBBH follows an eccentric orbit, then the changing radial distance leads to changing density. The density variation between two segments is quantified as $\Delta\rho_i = |\rho^{(i)} - \rho^{(i-1)}|$, representing the absolute difference of densities at adjacent observation segments.

In order to calculate the actual value of the $\Delta\rho_i$, we adopt a number of assumptions on the underlying accretion disk. For example, we employ the Sirko-Goodman (SG) thin disk model [48]. In the SG model, accretion disk could be partitioned into two distinct regions: the inner region is geometrically thin, with high angular frequency and temperature [60], the Toomre parameter $Q \approx \Omega^2/2\pi\rho \gg 1$ [61], and the outer region is a self-gravitating disk near marginal stability, where $Q \approx 1$ [61], with $\Omega = \sqrt{M_{\text{SMBH}}/r^3}$ as the angular velocity of the disk. In the outer region of the disk, the gas density profile $\rho(r)$ follows [48]: $\rho(r) = \Omega^2/2\pi = M_{\text{SMBH}}/(2\pi r^3)$. The power-law distribution of gas density in the accretion disk allows the density difference $\Delta\rho_i$ to vary in different observation segments.

The key to recovering the density profile is to associate the density ρ with the corresponding radius r . Following an eccentric orbit around the central SMBH, the barycenter of the sBBH to the SMBH evolves as time $r(t)$, and its exact evolution is determined by the semi-major axis a and the orbit eccentricity e_{orb} . Therefore, by assuming that the density is closely linked to the radius and by monitoring the changing rate of environmental density, it is possible to determine the orbital elements, such as the orbital eccentricity.

For the precision of gas density $\delta\rho_i$ estimation, we approximate with the FIM method. While the uncertainty in radius roots in the uncertainty in the timing. For the convenience of calculation, throughout our analysis, we assume the gas density to be constant during the i -th three-month period ρ_i , and there must be a moment \bar{t}_i when $\rho(\bar{t}_i) = \rho_i$, so that an effective constant density can explain the actual accumulated phase shift due to the changing gas density. Since in practice we do not know the exact time, we use the mid-time t_i^{mid} to approximate, and we denote the difference between \bar{t}_i and t_i^{mid} as Δt_i . We take σ_t , the standard deviation of the 20 Δt_i , to indicate the timing uncertainties. Combined with the determined orbit, the timing uncertainties can be translated into radius uncertainties.

We combine all the previous models to determine both the sBBH orbital elements (a , e_{orb} , ϕ_0), where ϕ_0 is the initial orbital phase), as well as the disk density profile parameters (α , M_{SMBH}) using the sequential observation of the sBBH inspiral waveforms $\rho = [\rho_1 \pm \delta\rho_1, \rho_2 \pm \delta\rho_2, \dots, \rho_{20} \pm \delta\rho_{20}]$ and the corresponding observation time $\mathbf{t} = [t_1 \pm \sigma_t, t_2 \pm \sigma_t, \dots, t_{20} \pm \sigma_t]$. We assume the estimation of the gas density and the time are statistically independent; therefore we construct the likelihood

function $P(\rho, \mathbf{t} | \bar{\theta})$ as:

$$-\frac{1}{2} \log P(\rho, \mathbf{t} | \bar{\theta}) = \sum_i \frac{(\rho_i - \rho(t_i, \bar{\theta}))^2}{2\delta\rho_i^2} + \sum_i \frac{(t_i - \bar{t}_i)^2}{2\sigma_t^2}, \quad (2)$$

where $\rho(t_i, \bar{\theta}) = \rho_0[r(t_i, a, e_{\text{orb}}, \alpha, M_{\text{SMBH}}, \phi_0)/r_0]^{-\alpha}$, $r_0 = 350r_s$ [26], $r_s \equiv 2M_{\text{SMBH}}$ is the Schwarzschild radius of central SMBH. Time series $t_i, i = 1, 2, \dots, 20$ are obtained from the GW observation segments, and the time-dependent radial distance r can be obtained by $(a, e_{\text{orb}}, \alpha, \phi_0)$. Finally, we can construct the posterior function from the likelihood and prior as Thus, we adopted χ^2 as our likelihood function $\mathcal{L}(\bar{\theta})$ to calculate the posterior distribution of $\bar{\theta} = a, e_{\text{orb}}, M_{\text{SMBH}}, \phi_0$. $P(\bar{\theta})$ is the prior of the parameters $\bar{\theta}$

$$P(\bar{\theta} | \rho, \mathbf{t}) \propto P(\bar{\theta}) P(\rho, \mathbf{t} | \bar{\theta}) \quad (3)$$

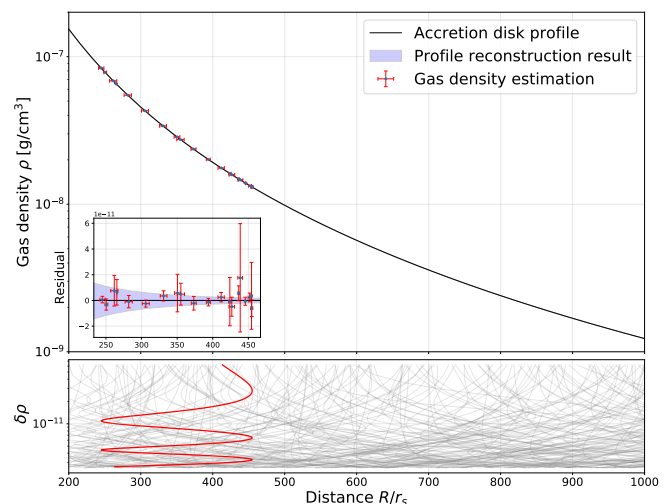


FIG. 2: The upper panel shows the injected (black line, SG model) and recovered (blue shaded region) disk density profile with an example event. Dots and error bars indicate the estimate of gas density and radial distance of the 3-month segments. The uncertainties are so small that we highlight the difference between the injection and the recovery in the zoomed-in panel. The lower panel shows the evolution of the gas density precision $\delta\rho$ for a population (grey) and the example (red) GW190521-like event.

In Fig. 2, we present our reconstruction ability on the density profile of the AGN disk. We simulate the data ρ, \mathbf{t} by adopting a $10^8 M_\odot$ central SMBH and a semi-major axis $a \sim 350r_s$. This combination lead to a period $T = \sqrt{4\pi^2 a^3/GM_{\text{SMBH}}} \approx 1.816$ yrs. The orbital eccentricity of the sBBH barycenter e_{orb} is set to 0.3. We then obtain the posterior through `emcee`.

In the upper panel, we plot the 20 estimates of the environmental densities, with the horizontal axis indicated by the radius during the three-month observation time. The density is shown together with their uncertainties $\rho_i \pm \delta\rho_i$

with error bars. In the horizontal axis, we show the radial distances of the sBBH system to the central SMBH, $r_i \pm \Delta r_i$ in the Schwaichii radius r_s unit. This is not the direct observables, but we convert the timing information to radius for better visualizations. According to the posterior, we also draw the uncertainties of the disk density profile with blue shaded regions. However, the uncertainty is too small, and we provide a zoomed-in subplot within to highlight the precision, using the blue shaded region to indicate the 90%CI of the residual between the recovered and the disk profile. From the plot we can observe that the AGN disk profile can be constrained with a precision generally better than $2 \times 10^{-11} \text{ g/cm}^3$. In the bottom panel, we show the evolution of estimation precision $\delta\rho$ (assuming a sliding 3-month window around) for a population of events. All of them are assuming the same GW190521-like binary parameters, but with varying (a, e_{orb}) combinations around the SMBH. The example event adopted in the upper panel is highlighted in red. We can observe that as the sBBH continues to spiral in, it decouples from the surrounding gas, so that the uncertainty increases.

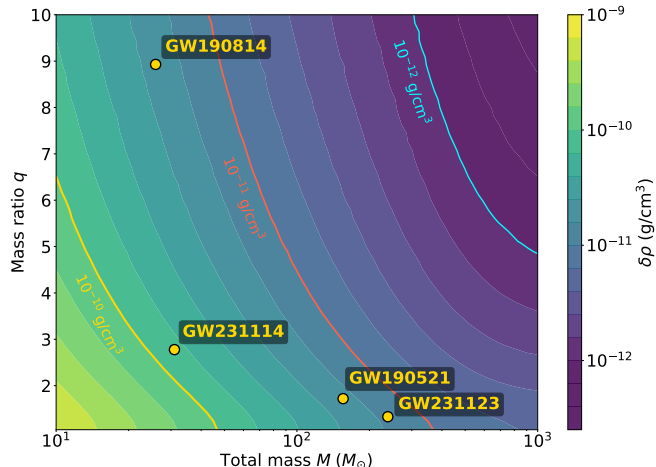


FIG. 3: The estimate precision $\delta\rho$ across sBBH systems with different total mass M and mass ratio q with the 3-month observation (solid lines). $\delta\rho$ equal to $10^{-12}/10^{-11}/10^{-10} \text{ g/cm}^3$ are shown with blue/red/green lines, respectively. The yellow dot represents the estimated precision of the gas density considering a GW190521-like event in 3 months.

We further study how the precision of our gas density inference varies across different mass parameters of sBBH systems. As shown in Fig. 3, heavier and more asymmetric sBBHs (higher total mass M , higher q) impose significantly tighter constraints on the ambient environment density. The enhanced precision enables the probing of a wider radial range in accretion disks: even for systems located farther from the disk center $> 10^3 r_s$, where the actual gas density variation between each 3-month segment become mild ($\Delta\rho \leq 10^{-10} \text{ g/cm}^3$) — the high measurement accuracy $\delta\rho \sim 10^{-12} \text{ g/cm}^3$ remains

sufficient to resolve such subtle variations ($\delta\rho < \Delta\rho$). The recent detection of high-mass systems in GWTC-4, such as GW231123 [25], which contains individual black holes exceeding $100 M_\odot$, has better potential in probing AGN disk profile, as such systems reside squarely in the high-sensitivity region of the parameter space. Besides, we plot two GW sources (GW190814[62],GW231114[63]) which have relative larger mass ratio q .

Conclusion - In this work, we have demonstrated for the first time that sequential GW observations by space-borne detectors can be used to reconstruct the density profiles of AGN disks. By achieving unprecedented resolution down to $\delta\rho \sim 10^{-11} \text{ g/cm}^3$ via Bayesian inference (Fig. 1), and by leveraging TianQin’s long-term observing capability, our method can trace systematic changes in the ambient density surrounding sBBHs, ultimately constraining the global disk profile with a relative accuracy on the order of $2 \times 10^{-11} \text{ g/cm}^3$. Furthermore, we have shown that this sensitivity is enhanced for heavier and more asymmetric binary systems — as demonstrated by the detection of high-mass systems such as GW231123 [25], along with high mass-ratio sources like GW190814 [62] and GW231114 [63], which exemplify the practical applicability of our approach.

In this letter, we present an approach that is currently applicable to the AGN disk model with a fixed power-law density distribution ($\rho \propto r^{-\alpha}$). Beyond DF effect, we acknowledge potential contributions from other environmental effects (gas accretion, acceleration of central black holes), which temporarily lie below detection thresholds of space-borne GW missions. Moreover, our method will be well-suited for probing ambient environment properties with next-generation space-borne gravitational-wave detectors offering higher sensitivity, such as DECIGO [64].

This methodology will expand multi-messenger observation coordination with TianQin, LISA, and other EM observatories. It will help reveal the deep connections between supermassive black hole accretion and galaxy evolution.

Xiangyu thanks Enrico Barausse for his great help with learning the corresponding gravitational wave environmental effect knowledge and the program in this project. Jiandong Zhang and Jianwei Mei also contributed a meaningful discussion of our work. This work has been supported by the National Key Research and Development Program of China (No. 2023YFC2206700), the Natural Science Foundation of China (Grant No. 12173104), the Natural Science Foundation of Guangdong Province of China (Grant No. 2022A1515011862), and the Fundamental Research Funds for the Central Universities, Sun Yat-sen University.

^{*} Corresponding author: shichf6@mail.sysu.edu.cn
[†] Corresponding author: huyiming@mail.sysu.edu.cn

[1] M. J. Rees, Ann. Rev. Astron. Astrophys. **22**, 471 (1984).
[2] A. C. Fabian, Ann. Rev. Astron. Astrophys. **50**, 455 (2012).
[3] J. Kormendy and L. C. Ho, Ann. Rev. Astron. Astrophys. **51**, 511 (2013), 1304.7762.
[4] Event Horizon Telescope Collaboration, K. Akiyama, A. Alberdi, W. Alef, K. Asada, R. Azulay, A.-K. Bacsko, D. Ball, M. Baloković, J. Barrett, et al., Astrophys. J. Lett. **875**, L1 (2019).
[5] Event Horizon Telescope Collaboration, K. Akiyama, A. Alberdi, W. Alef, J. C. Algaba, R. Anantua, K. Asada, R. Azulay, U. Bach, A.-K. Bacsko, et al., Astrophys. J. Lett. **930**, L12 (2022).
[6] W. A. Baan, T. An, C. Henkel, H. Imai, V. Kostenko, and A. Sobolev, Nat. Astron. **6**, 976 (2022), ISSN 2397-3366.
[7] G. A. Shields, Nature (London) **272**, 706 (1978).
[8] K. A. Pounds, J. N. Reeves, K. L. Page, G. A. Wynn, and P. T. O'Brien, Mon. Not. Roy. Astron. Soc. **342**, 1147 (2003).
[9] B. C. Kelly, J. Bechtold, and A. Siemiginowska, Astrophys. J. **698**, 895 (2009), 0903.5315.
[10] C. J. Burke, Y. Shen, O. Blaes, C. F. Gammie, K. Horne, Y.-F. Jiang, X. Liu, I. M. McHardy, C. W. Morgan, S. Scaringi, et al., Science **373**, 789 (2021), 2108.05389.
[11] J.-J. Tang, C. Wolf, and J. Tonry, Nat. Astron. **7**, 473 (2023).
[12] M. Morris, Astrophys. J. **408**, 496 (1993).
[13] J. Miralda-Escude and A. Gould, Astrophys. J. **545**, 847 (2000).
[14] A. Generozov, N. C. Stone, B. D. Metzger, and J. P. Ostriker, Mon. Not. Roy. Astron. Soc. **478**, 4030 (2018).
[15] C. J. Hailey, K. Mori, F. E. Bauer, M. E. Berkowitz, J. Hong, and B. J. Hord, Nature **556**, 70 (2018), ISSN 1476-4687.
[16] K. Belczynski et al., Astron. Astrophys. **636**, A104 (2020), 1706.07053.
[17] S. Stevenson, A. Vigna-Gómez, I. Mandel, J. W. Barrett, C. J. Neijssel, D. Perkins, and S. E. de Mink, Nature Commun. **8**, 14906 (2017).
[18] R. Farmer, M. Renzo, S. E. de Mink, P. Marchant, and S. Justham, Astrophys. J. **887**, 53 (2019), 1910.12874.
[19] M. Mapelli, M. Spera, E. Montanari, M. Limongi, A. Chiappi, N. Giacobbo, A. Bressan, and Y. Bouffanais, Astrophys. J. **888**, 76 (2020).
[20] P. Marchant and T. Moriya, Astron. Astrophys. **640**, L18 (2020).
[21] S. E. Woosley and A. Heger, Astrophys. J. Lett. **912**, L31 (2021).
[22] D. D. Hendriks, L. A. C. van Son, M. Renzo, R. G. Izzard, and R. Farmer, Mon. Not. Roy. Astron. Soc. **526**, 4130 (2023).
[23] R. Abbott et al. (LIGO Scientific, Virgo), Phys. Rev. Lett. **125**, 101102 (2020).
[24] R. Abbott et al. (LIGO Scientific, VIRGO), Phys. Rev. D **109**, 022001 (2024).
[25] A. G. Abac et al. (LIGO Scientific, VIRGO, KAGRA) (2025), 2507.08219.
[26] M. J. Graham et al., Phys. Rev. Lett. **124**, 251102 (2020).
[27] R. Abbott et al. (LIGO Scientific, Virgo), Astrophys. J. Lett. **900**, L13 (2020).
[28] V. Cardoso and A. Maselli, Astron. Astrophys. **644**, A147 (2020).
[29] A. Toubiana et al., Phys. Rev. Lett. **126**, 101105 (2021).
[30] P. Dutta Roy, P. Mahapatra, A. Samajdar, and K. G. Arun, Phys. Rev. D **111**, 104047 (2025).
[31] A. Caputo, L. Sberna, A. Toubiana, S. Babak, E. Barausse, S. Marsat, and P. Pani, Astrophys. J. **892**, 90 (2020).
[32] A. Toubiana, S. Marsat, E. Barausse, S. Babak, and J. Baker, Phys. Rev. D **101**, 104038 (2020), 2004.03626.
[33] C. Bonvin, C. Caprini, R. Sturani, and N. Tamanini, Phys. Rev. D **95**, 044029 (2017).
[34] K. Inayoshi, N. Tamanini, C. Caprini, and Z. Haiman, Phys. Rev. D **96**, 063014 (2017).
[35] N. Tamanini, C. Caprini, E. Barausse, A. Sesana, A. Klein, and A. Petiteau, JCAP **04**, 002 (2016).
[36] S.-C. Yang, W.-B. Han, H. Tagawa, S. Li, Y. Jiang, P. Shen, Q. Yun, C. Zhang, and X.-Y. Zhong, Astrophys. J. Lett. **988**, L41 (2025), 2401.01743.
[37] G. Caneva Santoro, S. Roy, R. Vicente, M. Haney, O. J. Piccinni, W. Del Pozzo, and M. Martinez, Phys. Rev. Lett. **132**, 251401 (2024).
[38] J. M. Fedrow, C. D. Ott, U. Sperhake, J. Blackman, R. Haas, C. Reisswig, and A. De Felice, Phys. Rev. Lett. **119**, 171103 (2017).
[39] A. Sesana, Phys. Rev. Lett. **116**, 231102 (2016).
[40] S. Liu, Y.-M. Hu, J.-d. Zhang, and J. Mei, Phys. Rev. D **101**, 103027 (2020).
[41] A. Sesana, J. Phys. Conf. Ser. **840**, 012018 (2017).
[42] S. Liu, L.-G. Zhu, Y.-M. Hu, J.-d. Zhang, and M.-J. Ji, Phys. Rev. D **105**, 023019 (2022).
[43] S. Marsat, J. G. Baker, and T. Dal Canton, Phys. Rev. D **103**, 083011 (2021).
[44] A. Toubiana, S. Babak, S. Marsat, and S. Ossokine, Phys. Rev. D **106**, 104034 (2022).
[45] R. Buscicchio, A. Klein, E. Roebber, C. J. Moore, D. Gerosa, E. Finch, and A. Vecchio, Phys. Rev. D **104**, 044065 (2021).
[46] X. Lyu, E.-K. Li, and Y.-M. Hu, Phys. Rev. D **108**, 083023 (2023).
[47] L.-G. Zhu, L.-H. Xie, Y.-M. Hu, S. Liu, E.-K. Li, N. R. Napolitano, B.-T. Tang, J.-d. Zhang, and J. Mei, Sci. China Phys. Mech. Astron. **65**, 259811 (2022).
[48] E. Sirko and J. Goodman, Mon. Not. Roy. Astron. Soc. **341**, 501 (2003).
[49] T. A. Thompson, E. Quataert, and N. Murray, Astrophys. J. **630**, 167 (2005), astro-ph/0503027.
[50] N. Jiang and Z. Pan, Astrophys. J. Lett. **983**, L18 (2025).
[51] I. Linial and B. D. Metzger, Astrophys. J. **957**, 34 (2023), 2303.16231.
[52] E. Barausse and L. Rezzolla, Phys. Rev. D **77**, 104027 (2008).
[53] E. Barausse, V. Cardoso, and P. Pani, Phys. Rev. D **89**, 104059 (2014).
[54] B. Kocsis, N. Yunes, and A. Loeb, Phys. Rev. D **84**, 024032 (2011).
[55] S. Khan, S. Husa, M. Hannam, F. Ohme, M. Pürrer, X. J. Forteza, and A. Bohé, Phys. Rev. D **93**, 044007 (2016).
[56] J. Luo et al. (TianQin), Class. Quant. Grav. **33**, 035010 (2016).
[57] H.-T. Wang et al., Phys. Rev. D **100**, 043003 (2019), 1902.04423.
[58] D. Foreman-Mackey, D. W. Hogg, D. Lang, and J. Good-

man, Publ. Astron. Soc. Pac. **125**, 306 (2013), 1202.3665.

[59] C. Cutler and E. E. Flanagan, Phys. Rev. D **49**, 2658 (1994).

[60] J. E. Pringle, Ann. Rev. Astron. Astrophys. **19**, 137 (1981).

[61] A. Toomre, Astrophys. J. **139**, 1217 (1964).

[62] R. Abbott et al. (LIGO Scientific, Virgo), Astrophys. J. Lett. **896**, L44 (2020).

[63] A. G. Abac et al. (LIGO Scientific, VIRGO, KAGRA) (2025), 2508.18082.

[64] S. Kawamura et al., Class. Quantum Grav. **28**, 094011 (2011).

Assessment of the constant-density approximation bias

We assess the systematic bias introduced by approximating the gas density as constant over each three-month observational segment, equal to its value at the segment’s midpoint. To quantify this bias, we develop a method to estimate the resulting uncertainty in the inferred radial distance $r_i(t)$ of the sBBHs in the accretion disk.

First, we define an effective mean density $\bar{\rho}_{\text{seg}}$ for

each three-month segment such that the integrated inner product under this constant density equals that under the true time-varying density $\rho_i(t)$. Specifically, $\bar{\rho}_{\text{seg}}$ satisfies:

$$\int_{f_0}^{f_{3\text{mon}}} \tilde{\phi}_{\text{DF}}(f, \bar{\rho}_{\text{seg}}) df = \int_{f_0}^{f_{3\text{mon}}} \tilde{\phi}_{\text{DF}}(f, \rho_i(t(f))) df, \quad (4)$$

where the time-frequency relation $t(f) = -\frac{1}{2\pi} \frac{d\Phi}{df}$.

We then compute the time offset Δt between the instant when $\rho(t) = \bar{\rho}$ and the nominal midpoint t_0 . Using the phase-derived relation $t(f)$, we reconstruct the density variation over the full five-year observation. For each of the 20 segments, the offset Δt_i is calculated. The distribution of these offsets is modelled as Gaussian, and its standard deviation $\sigma_{\Delta t}$ can be estimated.

Finally, we convert the temporal uncertainty $\sigma_{\Delta t}$ into a radial uncertainty δr using the orbital kinematics of the binary. The final result reports the inferred radial location as $r_i \pm \delta r_i$, accounting for the systematic error introduced by the constant-density assumption.